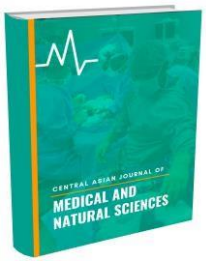

CENTRAL ASIAN JOURNAL OF MEDICAL AND NATURAL SCIENCES
https://cajmns.centralasianstudies.org/index.php/CAJMNS
Volume: 05 Issue: 04 | October 2024 ISSN: 2660-4159

Article

Synthesis and Characterization of Some New Imine Graphene Derivatives and Evaluation of Their Biological Activity

Abdul Wahed Abdul Sattar Talluh[1]*, Mohammed Jwher Saleh[2], Jamil Nadhem Saleh[3], Hamid Mohammed Saleh Al-Jubori[4]

1. Tikrit University, College of Basic Education, Shirqat, Tikrit, Iraq
2. Salah al-Din Education Directorate, Iraq
3. Salah al-Din Education Directorate, Iraq
4. Tikrit University, College of Basic Education, Shirqat, Tikrit, Iraq

* Correspondence: altlwhbdalwahd@gmail.com

Abstract: This study aimed to synthesize and characterize new imine graphene derivatives and evaluate their biological activity. Various nanoderivatives of graphene oxide were prepared and functionalized with symmetrical triazoles and amines through reactions involving oxidizing and acidic agents. The synthesis process included chemical exfoliation to create graphene oxide (GO), reduction of GO to reduced graphene oxide (RGO), and further functionalization with thiocarbohydrazide and triazoles. The resulting compounds were characterized using FT-IR, XRD, and SEM. Biological activity was tested against gram-positive Staphylococcus epidermidis and gram-negative Klebsiella pneumoniae bacteria. The synthesized compounds showed significant antibacterial activity, demonstrating their potential as antimicrobial agents.

Keywords: Graphene Oxide, Graphene, Triazole, Thiocarbodihydrazide, Imine, XRD, SEM, Biological activity

1. Introduction

Graphite is one of the materials available in nature and another form of carbon, each carbon atom is linked to three other carbon atoms within the same stereo plane, as is the geometric shape in aromatic hydrocarbons [1]. Graphene is a two-dimensional carbon sheet with a hexagonal crystal structure, and it is the thinnest material known to date, with an average diameter of only one carbon atom [2]. Therefore, it is considered one of the more efficient electrical conductors than copper, and it is one of the best heat conductors. In addition to being completely transparent and due to its high transparency, this led to an expansion of its use in the manufacture of touch screens and photovoltaics [3, 4]. Prepared from chemical vapor deposition and reduction of graphene oxide using hydrazine, which has been the most common method since 1958 when it was discovered by two scientists Hammer and Furman [5, 6]. Graphene has unique properties that make it an interesting material for many applications such as energy storage and electronic devices [7]. It is also used as a single thin layer in coatings and is also used in the production of modified surfaces [8]. Graphene is of limited use due to its high cost, and it also has optical applications as it consists of a two-dimensional thin layer that can be used in optical electronic devices such as transistors [9].

Triazoles are weak bases and have high stability, especially the analogs of S-Triazole, and its important derivatives are imines, which are prepared in different ways, the most famous of which is its reaction with aldehydes and ketones in different media [10]. It has

Citation: Talluh, A. W. A. S., Saleh, M. J., Saleh, J. N., & Al-Jubori, H. M. S. Synthesis and Characterization of Some New Imine Graphene Derivatives and Evaluation of Their Biological Activity. Central Asian Journal of Medical and Natural Science 2024, 5(4), 272-290.

Received: 13th July 2024
Revised: 20th July 2024
Accepted: 27th July 2024
Published: 3rd August 2024

many applications such as its action as antibiotics, drugs, and dyes [11], and largely anti-cancer [12] and analgesic [13, 14]. Also, Triazoles have been used as corrosion inhibitors on solid carbon steels in acidic solutions and have demonstrated excellent stabilizing efficacy [15].

2. Experimental

Characterization

IR spectra were obtained using (FT-IR) (65 FT-IR Perkin Elmer Spectrophotometer) as well as a diffraction X-ray device (Shimadzu-XRD-6000) and Scanning Electron Microscopy (SEM).

Graphite chips (99.9%) were purchased from (China), sulfuric acid (H_2SO_4, 98%), Sodium nitrate ($NaNO_3$, 99%), hydrochloric acid (HCl, 37%), potassium permanganate ($KMnO_4$.99%), hydrogen peroxide (30%, H_2O_2), aqueous hydrazine ($N_2H_4.H_2O$, 60%).

Preparation of graphene oxide: GO (Hummer method)

A 600 ml beaker was submerged in an ice bath, to which 1.5 g of sodium nitrate and 46 ml of concentrated sulfuric acid were added while magnetic stirring was in place. One gram of graphite was added to the mixture after fifteen minutes, and it was increased progressively for ten minutes. Next, over the course of ten minutes, 6 g of potassium permanganate was progressively added to the mixture while maintaining a temperature below 20 °C.

Following the addition, the mixture was placed in the ice bath for five minutes. After that, it was taken out of the bath and allowed to swirl magnetically for two hours. Within twenty minutes, 46 milliliters of distilled water were added very slowly (using a dropper). After raising the temperature to 98 °C for 20 minutes, 300 ml of distilled water was added, and the mixture was left for 24 hours. After that, 140 ml of warm distilled water (50 °C) was added, and it was stirred for 10 minutes at room temperature. Next, 15 ml of 30% hydrogen peroxide was added, and it was stirred for 30 minutes. poured and collected once, after which the leftover product was rinsed five times (45 ml 5) with deionized water until the pH reached 7. Next, it was rinsed once with a 10% hydrochloric solution.

Preparation of Graphene oxide Reduced

One milliliter of hydrochloric acid and 0.1 grams of graphene oxide were added to a round flask that held 50 milliliters. The mixture was then stirred until it became homogenous, or clear and devoid of plankton. After that, one milliliter of hydrazine hydrate was added, and it was heated to 100 degrees Celsius for two hours while a reflex condenser was present. Following that, filtering was used to gather the RGO. The product was rinsed many times with deionized water in order to eliminate any remaining hydrazine. The product was dried at 100 °C in a vacuum oven. for twelve hours.

Preparation of Thiocarbodihydrazin (TCDH)

5 ml of carbon disulfide was added to a 100 ml round flask on an ice bath and 20 ml of hydrazine hydrate (80%) was added to it in drops within 10 minutes with continuous stirring, the reaction mixture was reflected for 30 minutes, a light yellow precipitate was formed, and the precipitate was collected by filtration and washed with ethanol. Until the color of the precipitate formed white, it was collected and recrystallized from distilled water and then dried at 70 °C until the weight was stable.

Preparation of 3-thiol-4-amino-1,2,4-triisol-graphene oxide reduced (RGO-TZ)

0.4 g of thiocarbohydrazide was mixed with 0.1 g of reduced graphene oxide in a heat-resistant flask. The mixture was heated in an oil bath by stirring in a glass rod for 10 minutes at 170 ° C. The product was cooled to room temperature, then the molten was treated with a 10% solution of sodium bicarbonate to get rid of the unreacted acid residue. The precipitate was filtered, washed with ethanol, and dried at 60 °C.

Preparation of RGO-TZ Imines

0.1 g of the prepared RGO-TZ derivative was mixed with 0.2 g of different aromatic aldehydes in a suitable and heat-resistant beaker without using a solvent. Heat the mixture while stirring gently until the nature and color of the reactants change. The product is collected and recrystallized in absolute ethanol.

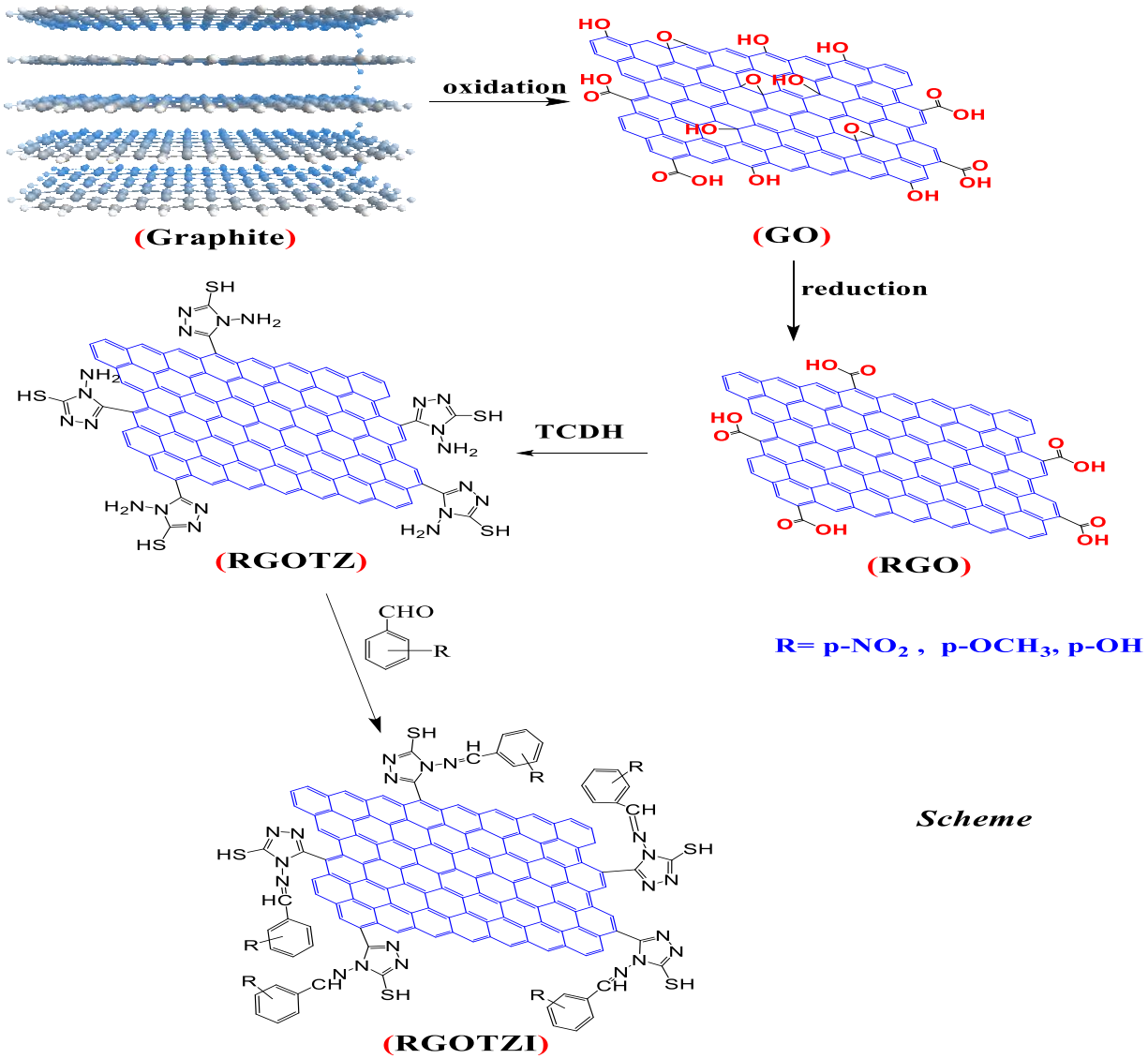

Scheme

Study of Biological activity

Gram-positive *Staphylococcus epidermidis* and Gram-negative *Klebsiella pneumoniae* were the two kinds of bacteria that were employed. The compounds were then produced in chemical solutions at concentrations of (0.0001, 0.001, and 0.01) mg/ml for each solid derivative, using DMSO as a solvent. The Mueller-Hinton agar medium should next be prepared by the manufacturer's instructions so that its biological activity may be examined [16]. In a conical flask, one liter of distilled water is added to the medium powder (38 g), and the mixture is heated until the powder dissolves [17]. The culture media is dissolved,

and the mixture is then autoclaved to sanitize it. The culture media is sterilized after cooling for fifteen minutes at 121 degrees Celsius and 1.5 bar of pressure [18, 19]. Transfer onto a platter and finish cooking. After putting the bacteria in the culture media, drill holes in the Petri plates using a cork drill, disinfect the holes with alcohol, and fill the holes with the prepared solution using a fine pipette [20]. A centimeter ruler was used to measure the width of the compound under study's inhibitory zone after it had been in the incubator for 24 hours at 37 degrees Celsius [21].

3. Results and Discussion

Preparation and diagnostics of graphene oxide nanoparticles

Graphite is the raw material for preparing graphene oxide (GO) from polycrystalline particles or granules that can be selected from natural and artificial sources. Natural graphite is the most common source for it [22], The rationale for this is that various structural flaws in natural graphite might function as catalysts for chemical processes [23].

The production of graphene oxide and subsequent reduction of graphene oxide via the Hummer method, which involved mixing sodium nitrate and oxidizing agents catalyzed with sulfuric acid and graphite in an aqueous medium, can be used to illustrate the potential reactions of the active groups in graphite's composition in the presence of oxidizing agents and acids [24, 25]. Inside the graphite crystals, the molecules of oxidizing agents (KMnO4) and acids permeate the layers. As a result, when the temperature is raised, the oxidation between the layers causes the layers to diverge, which causes the oxygen atoms to repel because of the partial or total repulsion of the layers.

The FT-IR of the nanographene oxide appeared distinct and broadband due to the overlapping hydroxyl alcoholic and carboxylate groups at (3434),

Table 1. Results of the FT-IR (cm^{-1}) for the nanographene oxide

Comp. NO.	Comp.	I.R. – KBr, υ – cm^{-1}					
		hydroxyl alcoholic and carboxylate groups	C=O	C-O carbonyl	C=C	C-O epoxide	C-H Alif.
A_1	N. G. O.	3434	1726	1221	1625	1051 1221	2820 2950

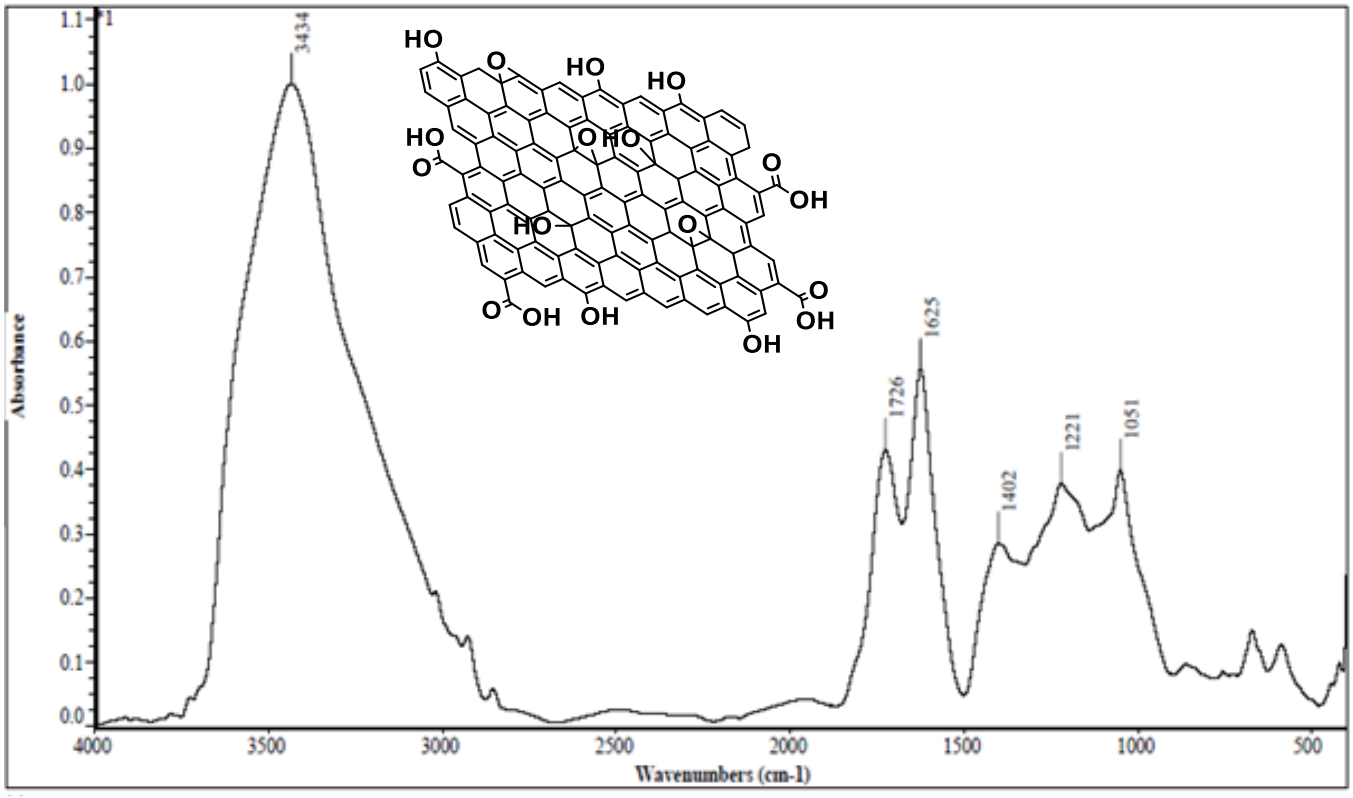

Figure (1) shows the FT-IR spectrum of graphene oxide.

From the observation of the SEM image of graphene oxide GO, we note the nanoscale thickness of the layer from the measurements on the image, as well as a comparison of the edges of the plate with the measurement and the color difference in the regions of one plate, which indicates the difference in the degree of oxidation depending on the peeling period and its duration for each plate.

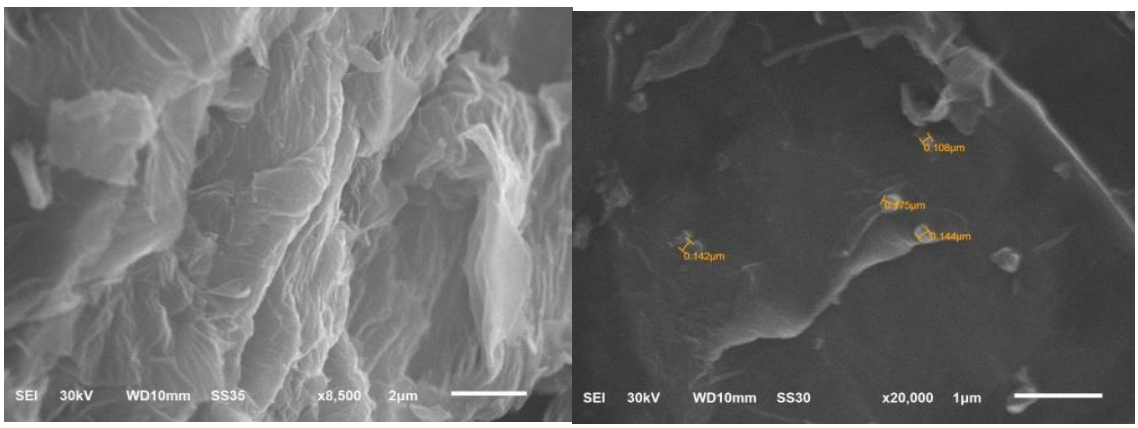

Figure 2. The SEM images of compound (A1)

Preparation of NRGO reductase graphene oxide nanoparticles (A2)

Reduced graphene oxide (RGO) was prepared from the reaction of graphene oxide with hydrazine hydrate (80%) ($NH_2NH_2.H_2O$).

Through the FT-IR spectrum, it was observed that the stretching of the epoxy group of reduced graphene oxide disappearance is represented by the C-O peak, which is attributed to the reduction process. Also, the stretching peak of (C=O) at (1724) cm $^{-1}$ was reduced, while the stretching of (C=C) at (1649_ 1487) cm^{-1} appeared.

This proves that the results of the reduction had formed a sp2 interaction in the carbon compositions [26], so, we conclude that the graphene sheets were formed during the process of graphene oxide reduction.

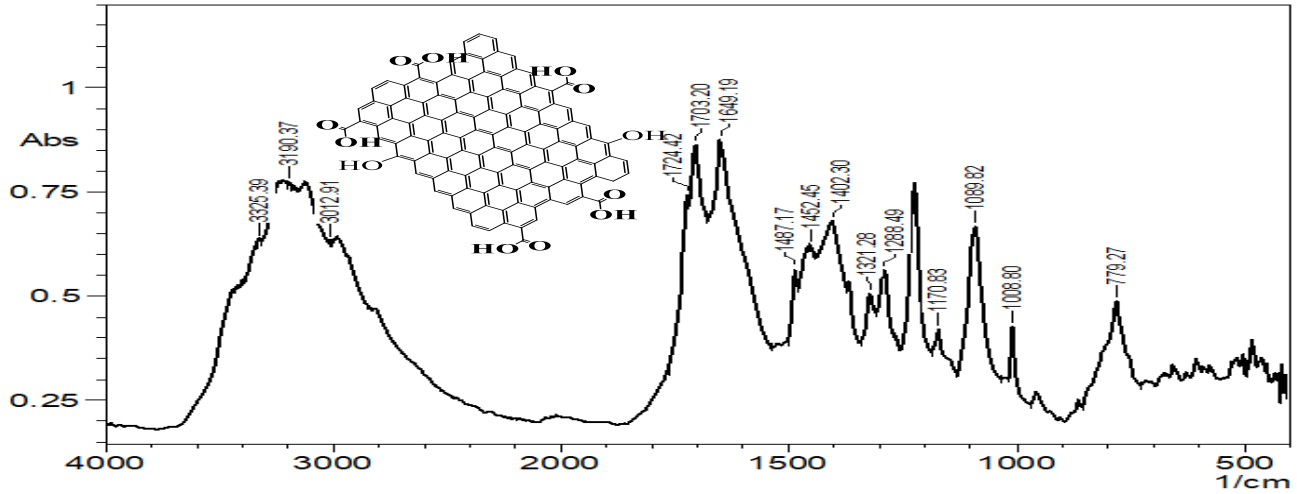

Figure (3): shows the FT-IR spectrum of graphene.

From the observation of the SEM image of RGO (reduced graphene oxide) prepared (a, b), we generally find that the morphology of the plates did not change much, but the purity of the plates compared to GO is observed, due to the elimination of oxidation pools and the varying distances, as well as the removal of water molecules trapped between the layers. The nanoscale thickness of the layers with twisted edges indicates an earlier flow of moisture during removal.

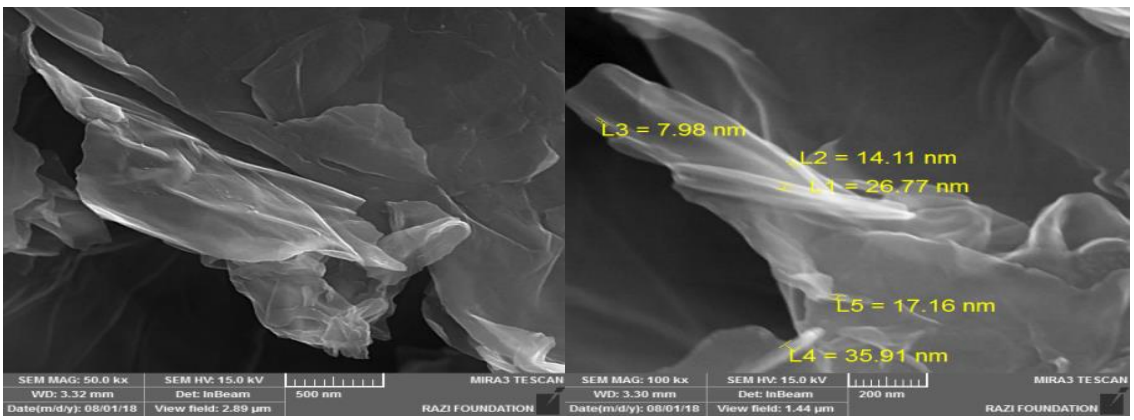

Figure 4. The SEM images of compound (A2)

Preparation and Diagnosis of Thiocarbudaihydrazide (TCDH)

Due to the yield (80%) of the distinctive crystals, thiocarbudaihydrazide was produced from a combination of carbon disulfide and aqueous hydrazine.

The infrared spectrum revealed a peak at (1284) cm^{-1} belonging to the stretching of the bond C = S in addition to the corresponding stretching frequency of the primary amine group (NH_2) at (3273, (3305) cm^{-1} respectively. These physical properties, such as color and melting point, were used to diagnose the product. Both the secondary amine stretching

peak and the group (NH_2) scissor bending frequency were seen at (3204) cm^{-1} and (1143-1140) cm^{-1}, respectively [27].

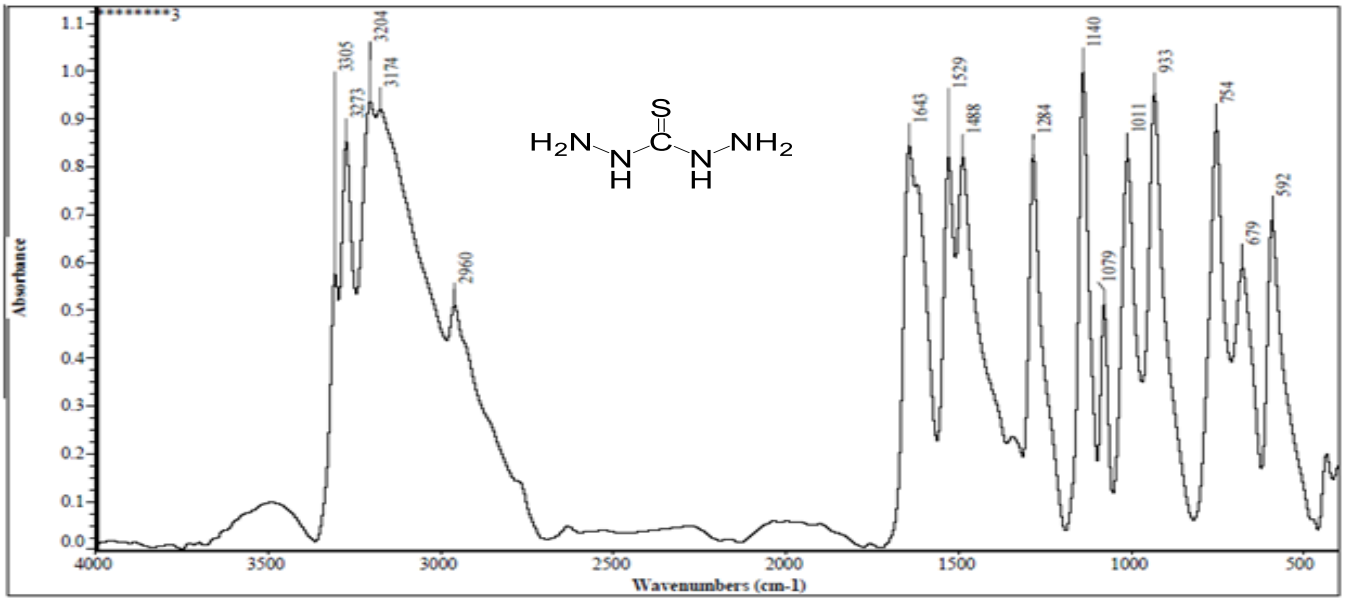

Figure (5) shows the infrared (FT-IR) spectrum of the compound TCDH)

Preparation and diagnostics of thiocarbudaihydrazine with reduced graphene oxide

The triazole derivative corresponding to the reduced graphene oxide containing the 1,2,4-triazole ring primary amine was prepared at the position No. (4) of the ring via a thermal smelting reaction in the solid state where the smelting at the melting point of TCDH is to pass the formation phase for 1-2 minutes. As it gave a good yield in a short time.

Because of the overlapping amine and alcohol, the FT-IR spectrum revealed a unique and broadband pattern hydroxyl groups at (3434) cm^{-1} as well as a peak at (2854, 2924) cm^{-1} attributable to the symmetric and asymmetric vibrations of the terminal (2CH) group respectively and the disappearance of the carbonyl group (C = O) at (1729) (cm^{-1}) evidence of the reaction, and it showed a peak at (1629) belonging to the right group (C = N), while it gave the bond C = C stretch peak at (1574) cm^{-1}) [28].

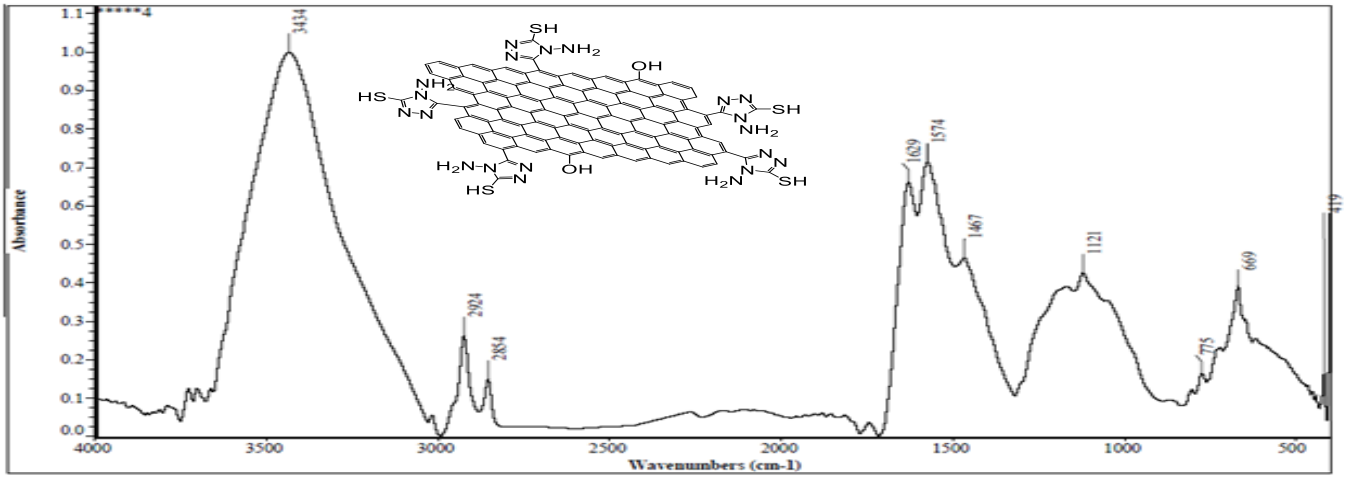

Figure 6: FT-IR spectrum of triazole-reduced graphene oxide (NRGOTZ)

From the observation of the morphological image of the graphene derivative (NRGOTZI) (a-c), containing the 1,2,4-triazole ring, we observe the increase in the porosity of the material and this supports the increase in the intermediate distances shown in the

XRD spectrum of the compound in Figure 7 as the zigzag surface indicates Peeling occurs due to the new polarization of the plate.

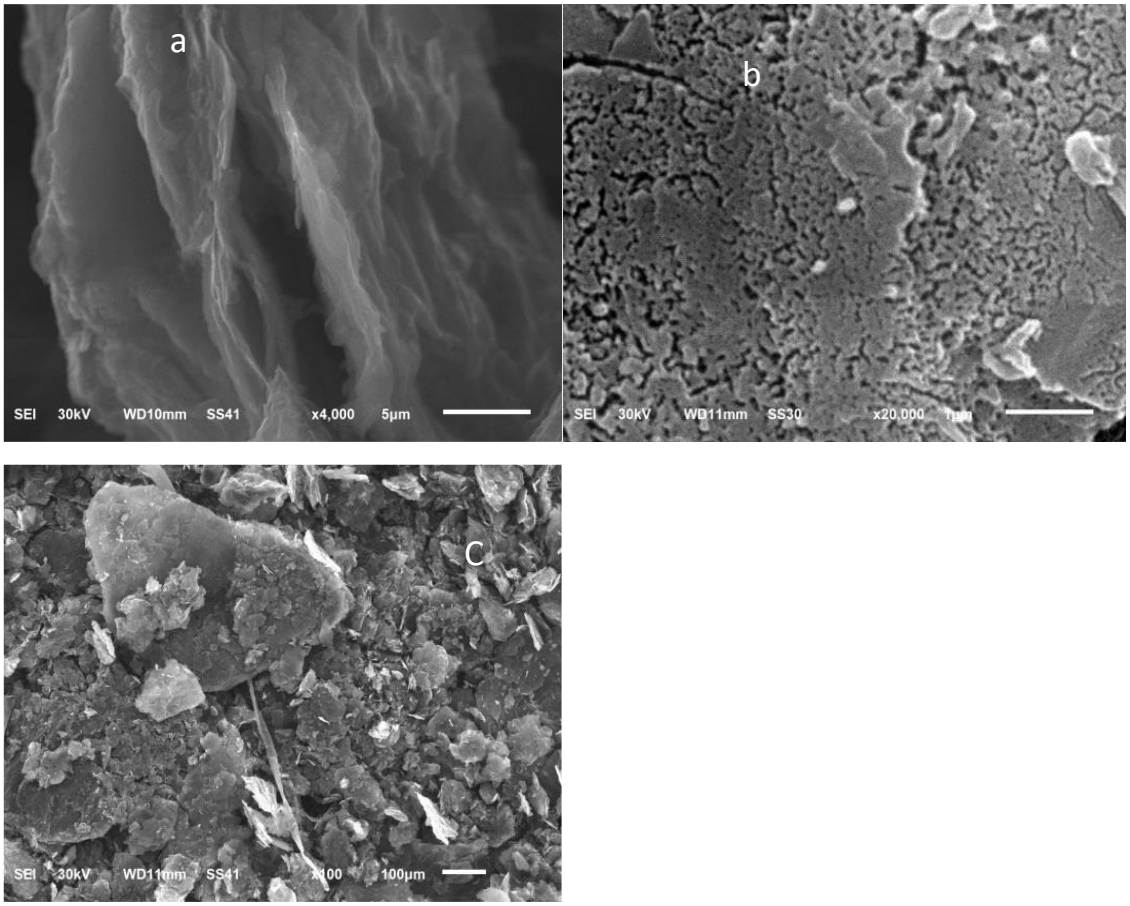

Figure 7. SEM images of compound (4)

Discussion of the preparation of amines corresponding to the compound (NRGOTZI) (5-7)

The amines corresponding to the prepared nanoparticles (NRGOTZI) were prepared by using the solid phase thermal fusing method for each of the amine terminal materials, which is NRGOTZI, and the used dehydrates. The reaction took place at a time of (8) minutes through a staining stage (1-2) minutes, and with a good yield (70%) upon fusion or homogeneous mixing.

The prepared compounds (5-7) were diagnosed with some physical properties and an infrared spectrum. The FT-IR spectrum showed new absorption peaks of the amine conjugate stretch (C = N) within the range (1631) cm^{-1}. Also disappearance of the primary amine stretch peak (NH_2) at (3395-3432) cm^{-1}, in addition to an increase in the absorption intensity of the stretch peak (C = N) compared to the compound spectrum (NRGOTZ).

Also, a pack of benzyldinates was shown, such as C-Cl at (1079) cm^{-1} for compound (5) and C-Br at (1200) cm^{-1} for compound (7). As in Table 2 and Figures 8-10.

Table 2. The values of the FT-IR for compounds [5-7]

Comp NO	**IR, ν, (cm^{-1})**						
	OH	=C-H	C=C	C=N	C-O	C-H	**Others**

5	3431	3017	1574	1631	1120	2924	--
			1494		1260	2854	
6	3429	3041	1591	1608		2918	NO2,
			1556			2847	1514,1330
7	3333	3020	1514	1602	1168	2980	--
			1456			2825	

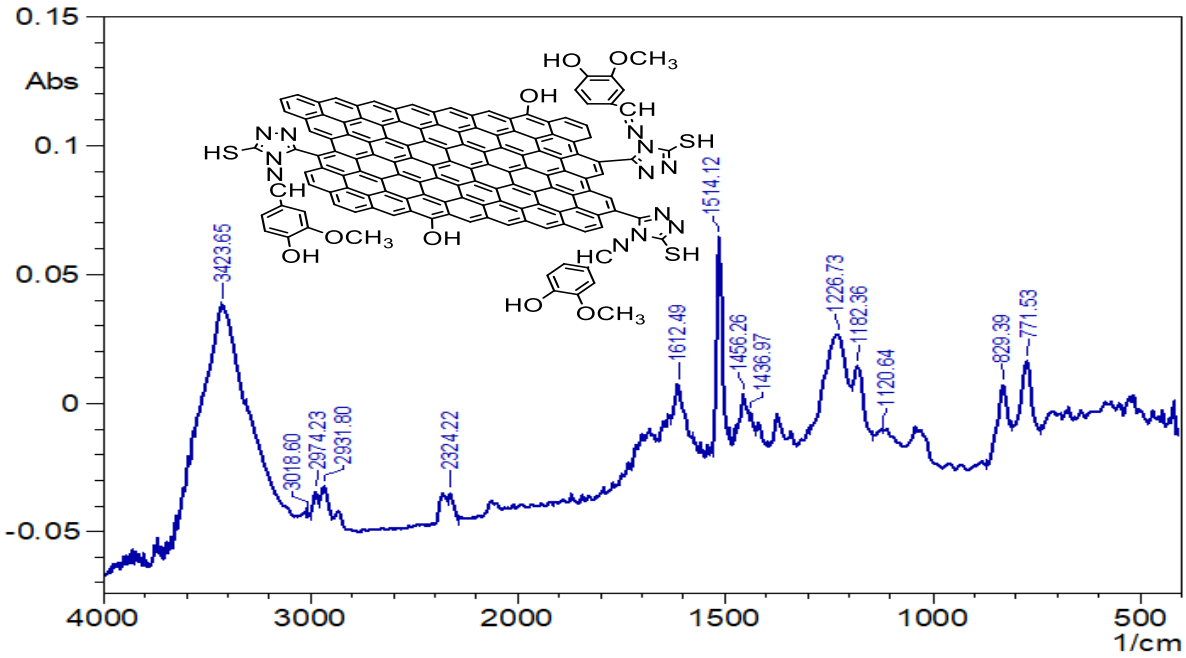

Figure 8. The (FT-IR) spectrum of (5) compound

The SEM images of the derivative (8) show a slight thickness of the layers up to (0.5) Nm (a), and this indicates the ease of melting the material and entering it between the layers, although the distance remains close to the rest of the derivatives in the XRD spectrum. (Figure 3-4)

The SEM of the derivative (8) also showed the presence of some stratigraphic groupings with an average nanoscale size of minutes (b). This may be attributed to the ability of the compensated groups such as OCH3, and OH on the benzene ring to form hydrogen bonds with clear clusters appearing on the edges (c) and some of them on the plate.

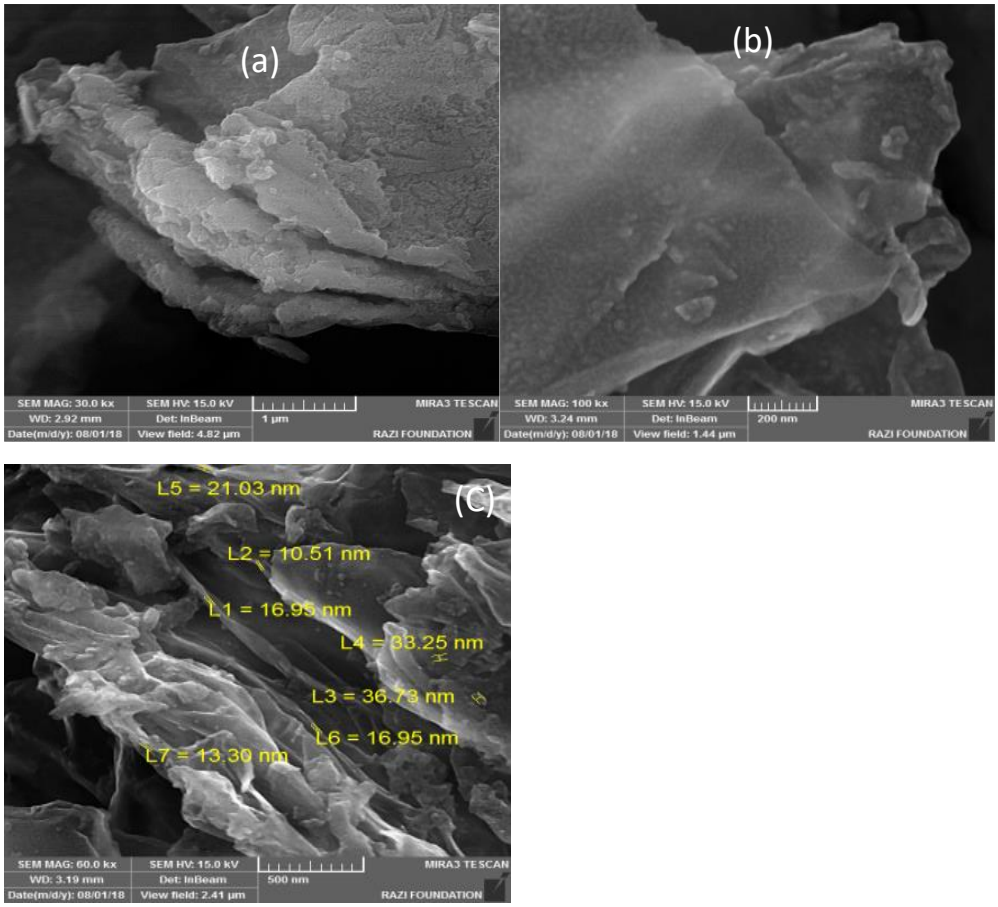

Figure 9. SEM images of compound (5)

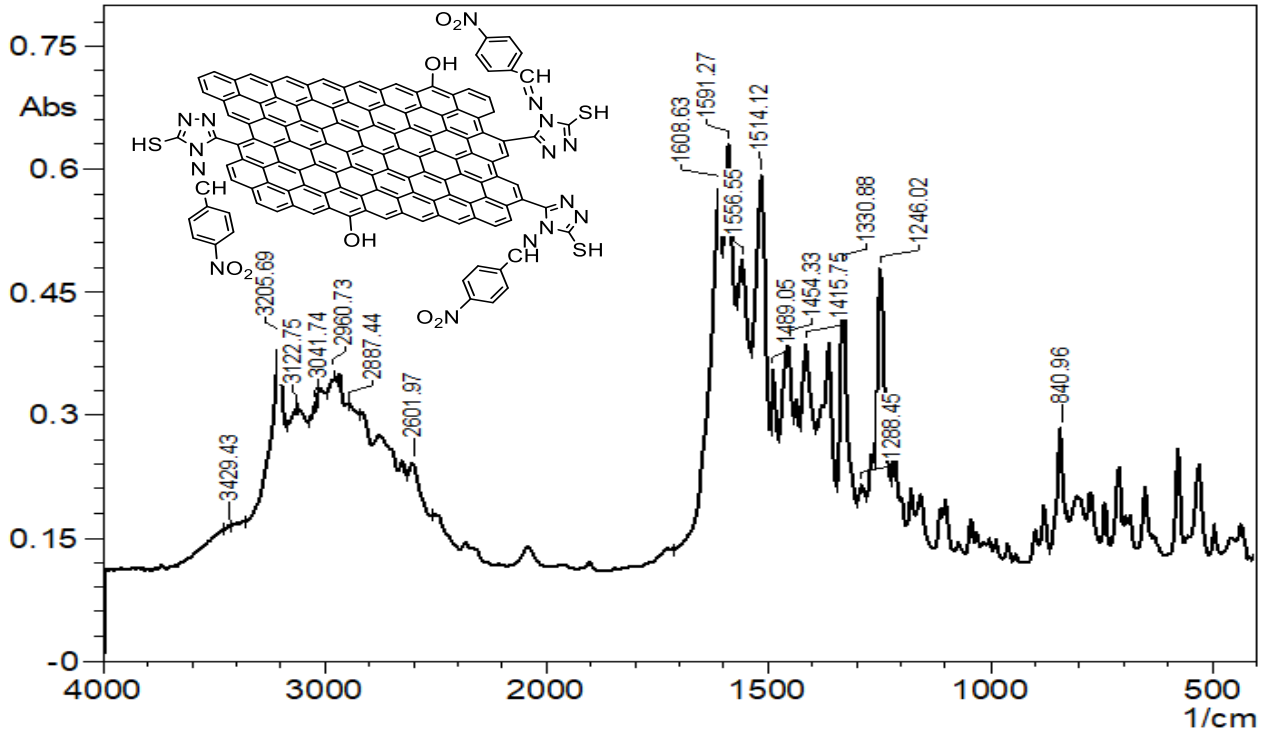

Figure 10. The (FT-IR) spectrum of (6) compounds

It was observed from the SEM image of the compound (9), a) that the large distances between the stratigraphic clusters reach, according to the scale, a range of 1-1.5 micrometers. Figure (9) (b) shows the polarization of the layer as it sometimes turns on itself, in cases of monolayer, Edge aromatic accumulations were more evident in (c) where they are lined with accumulating filaments with unaffected edges indicating that the triazole groups are not evenly distributed over the edges.

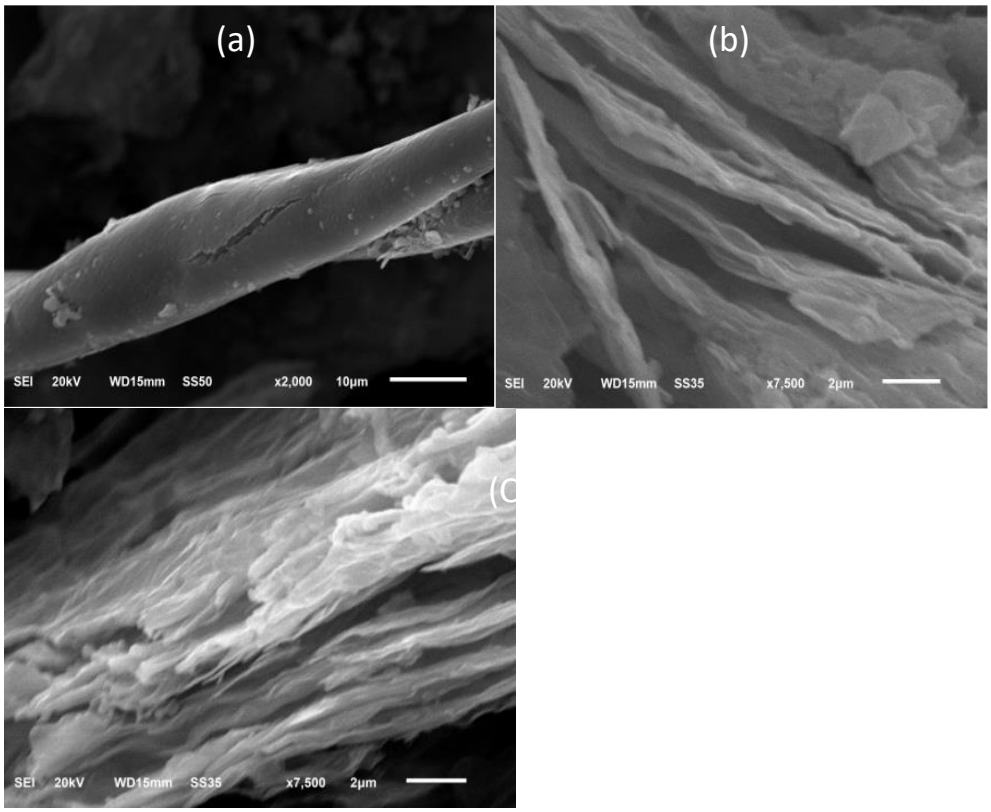

Figure 11. SEM images of compound (6)

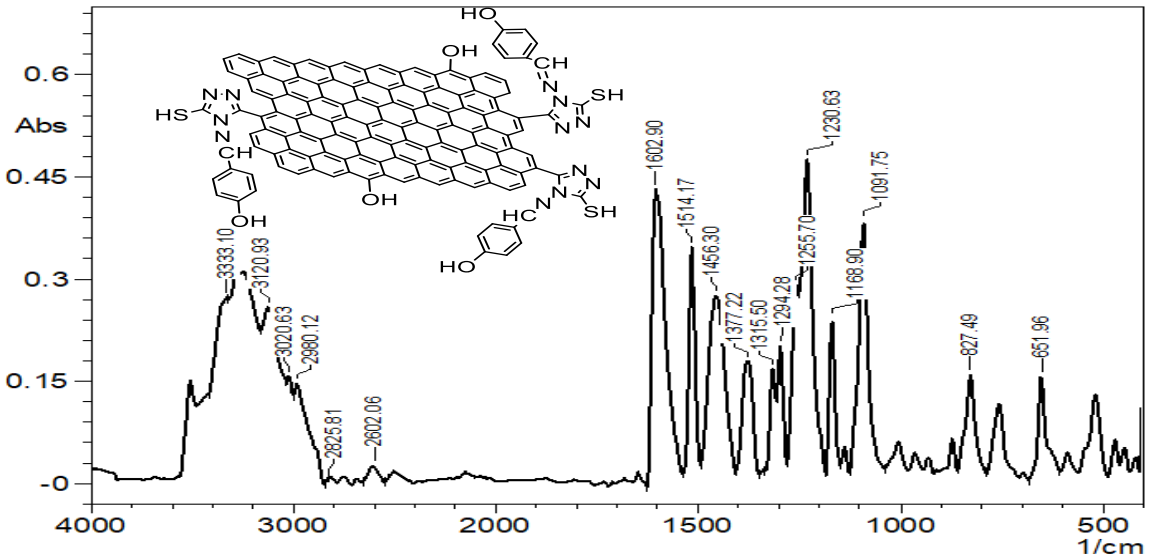

Figure 12. The (FT-IR) spectrum of the (7) compound

Through the morphological images of the derivative 10, it was observed that the distances between the clusters appeared while maintaining the peeling, and the aromatic parts gathered on the edges (a) and on the surface (b) (c) with a more distributed ratio, and

this indicates a greater ability to bond, which may be attributed to the formation of inter-hydrogen bonds with increasing potential particle size. As in Figure (13).

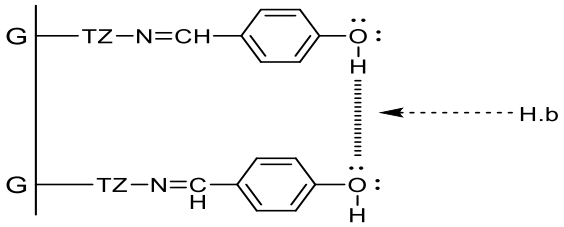

Figure 13. Hydrogen bonds between plates

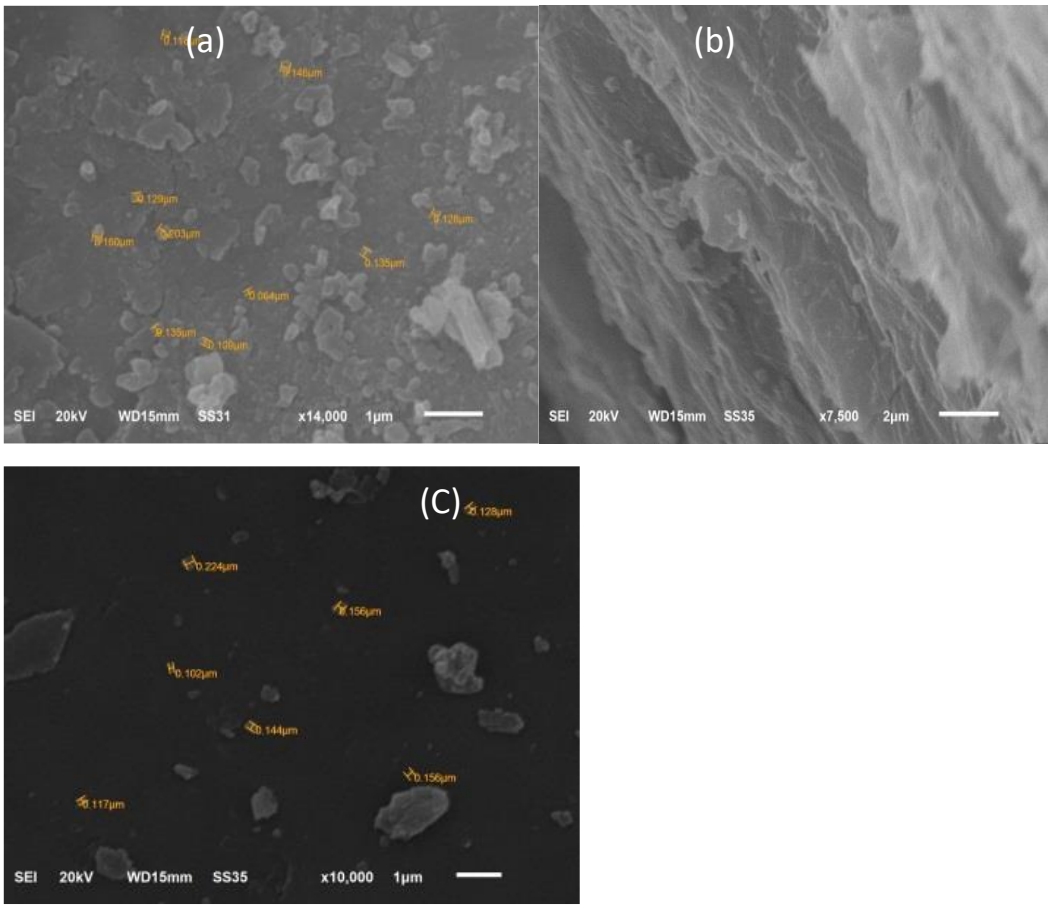

Figure 14. SEM images of compound (7)

Diagnosis of graphene oxide by X-ray diffraction spectrum

The main peak of the graphene oxide was revealed by the X-ray diffraction measurement to be a high-intensity peak at angle 2 θ = 12.33 with an interchange distance d = 7.17 A˚. Other peaks were also observed at angle 2 θ = 10.55 A˚ with an interchange distance of 8.37 A˚ and at angle 2 θ = 9.80 A˚with an interchange distance of 9.017 A˚. The average size of the nanoparticles was 6.11 nm, as illustrated in Figure (15).

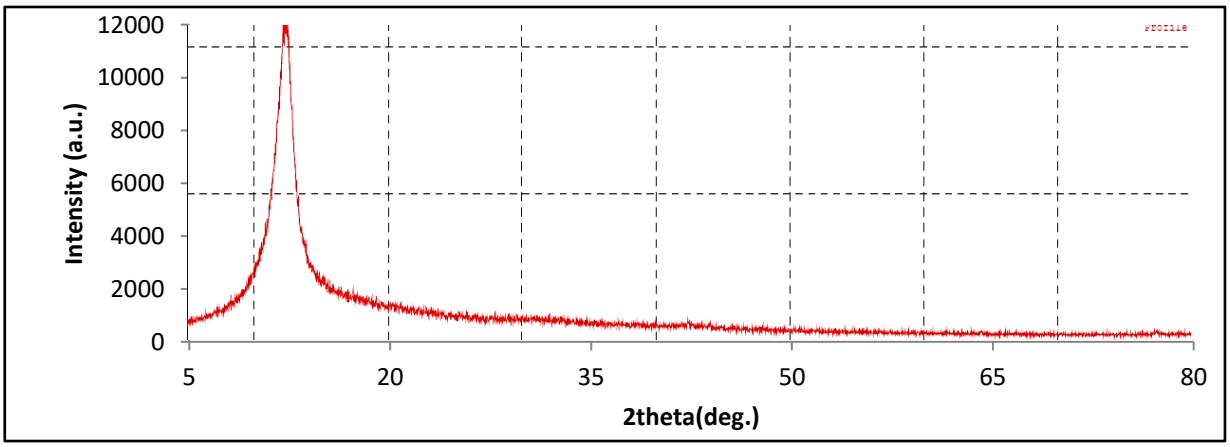

Figure 15. Graphene oxide X-ray diffraction spectrum (XRD)

X-ray diffraction measurement of RGO:

The decreased graphene oxide's X-ray diffraction measurement revealed a broad peak at angle 2 θ = 29.50^ and exchange distance d = 3.02 A˚. The test revealed another peak at angle 2θ = 32.59˚ with an interchange distance of 2.74 A˚ . This interface distance is significantly less than the interlayer distance in graphene oxide. The average size of the nanoparticles was 23.01 nm, and the measurement also revealed another peak at angle 2 θ = 28.26 ˚ with an intermediate distance, 3.15 A˚.

The disappearance of the peak at the angle 2θ = 12.33˚ in graphene oxide indicates the reduction of most of the oxygen groups and their conversion to the reduced graphene oxide in addition to the removal of water molecules penetrated between the plates, which were associated with the hydrogen bonds with the oxygen atoms of the oxide groups, as shown in Figure (16).

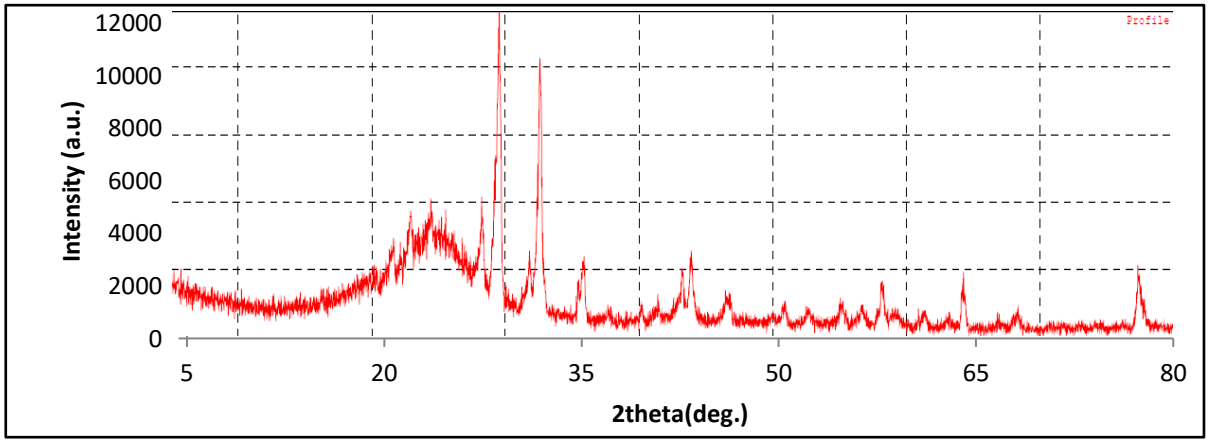

Figure 16. XRD spectrum of reduced graphene oxide (RGO)

X-ray diffraction measurement of the compound (RGOTZ):

RGOTZ powder X-ray diffraction measurement showed several peaks starting from (2Θ = 26.96º 25.07º, 25.76º) for the separation distances (3.54) Aº, (3.45) Aº, (3.30) Aº, respectively, and the average size of the nanoparticles was 5.67 nm. as shown in Figure (17).

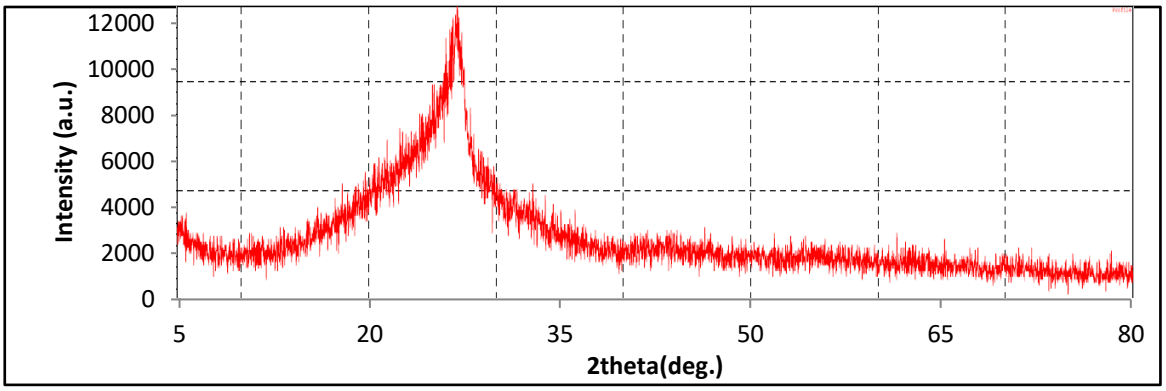

Figure 17. XRD spectrum of compound (4)

X-ray diffraction measurement of RGO-TZ:

The X-ray diffraction measurement of the compound (8, NRGOTZI) showed several peaks starting from 2Θ = 26.98° 25.84°, 25.07° for separation distances (3.30) A°, (3.44) A°, (3.54) A°, (3.30) A°, respectively, the average size of the nanoparticles was 5.35, as shown in Figure (18).

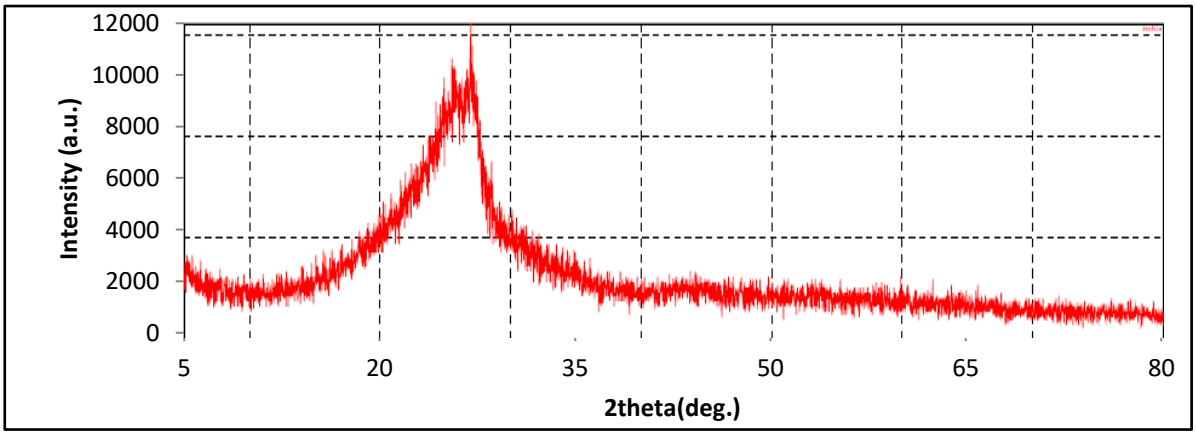

Figure 18. XRD spectrum of compound (5)

The X-ray diffraction measurement of the compound (9, NRGOTZI) showed several peaks starting from 2Θ = 27.44° 17.26°, 24.18° for separation distances (3.24) A°, (5.13) A°, (3.67) A°, respectively, and the average size of the nanoparticles was 36.76 nm, as shown in Figure (19).

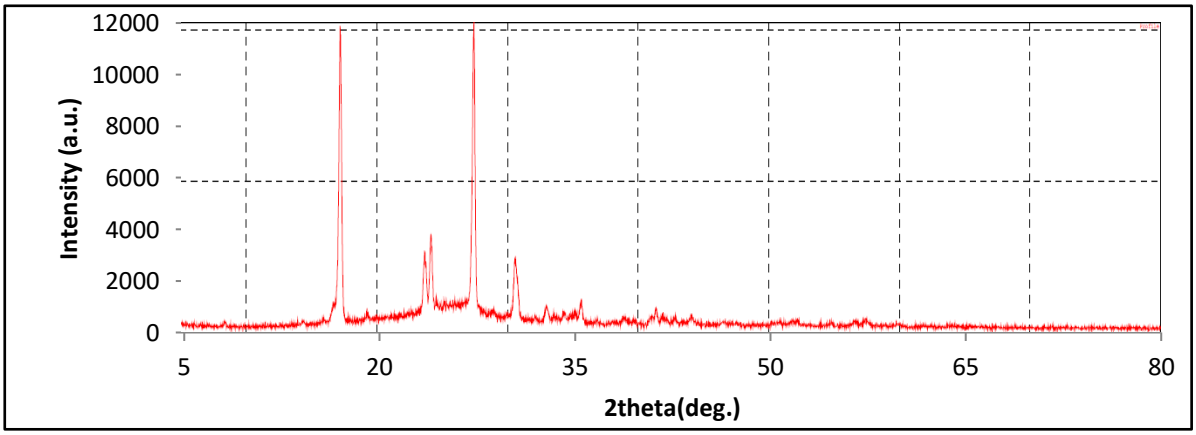

Figure 19. XRD spectrum of compound (6)

The X-ray diffraction measurement of the compound (10, NRGOTZI) showed several peaks starting from 2Θ = 26.82° 25.92°, 24.53° for the separation distances (3.32) A°, (3.43) A°, (3.62) A°, respectively, and the average size of the nanoparticles was 4.13 nm, as shown in Figure (20).

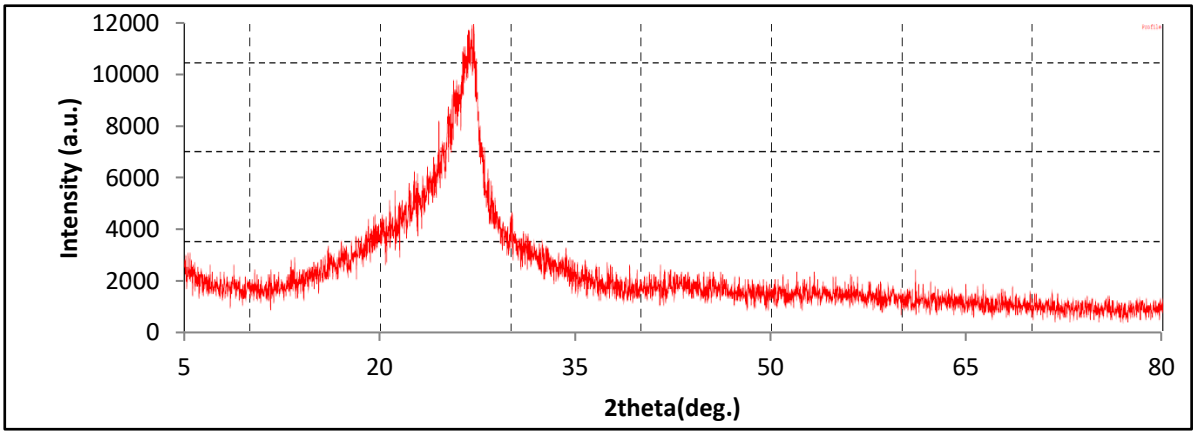

Figure 20. XRD spectrum of compound (7)

Measurement of corrosion inhibition of some prepared compounds

In this method, medium carbon steel is used, which is used in many industrial fields, and it is in direct or indirect contact with sulfuric acid, where all experiments were done using the lost weight technique. To make sure of the action of these inhibitors, a concentration of the inhibitor was taken and the corrosion was compared with the Blank solution used without adding an inhibitor to the metal surface after immersion in the retarder prepared with sulfuric acid. It was observed that the covering layers formed on the surface of the metal through the adsorption process and thus worked to inhibit the corrosion of medium carbon steel with the acid. The difference in corrosion was observed through the difference in the lost weights.

In this work, we selected two different compounds (TCDH, RGO-TZ) to test the inhibition of corrosion of medium carbon steels in sulfuric acid.

In both the presence and absence of the inhibitor, as well as in the presence of the inhibitor at a concentration of 0.2 g and a volume of the inhibitor, the samples were submerged in sulfuric acid electrolytic solutions at room temperature. The samples were immersed in the acidic solution for a maximum of twenty-four hours, during which time the weight per unit area was used to measure the change.

The corrosion efficiency was calculated using the following weighing equation:

$$IE\% = \frac{Wu - Wi}{Wu} * 100\%$$

Wi: Weight lost with an inhibitor in (μg / cm².h) units

Wu: weight lost without inhibitor in units (μg/ cm².h)

Wu, Wi: - lost weight (μg / cm².h) with and without inhibitor, respectively

The following data show the effect of the period of exposure to an acid solution (H2SO4) on the lost weight of the samples in the presence and absence of the inhibitor, at room temperature and shows the clear difference between the weight lost from the medium carbon steel sample in the acid solution without the inhibitor and the weight lost from the steel samples in the acid solution in the presence of the inhibitor. Especially at high levels of inhibitor, as the highest rate of inhibition of the compound (3) reaches (78%) in the first 5 minutes, and then begins to slow gradually until it reaches (17%) after 24 hours.

This is due to the efficiency of the molecule on the one hand in conjunction with the acid due to its basic characteristic of having non-participating electron pairs on the S and N atoms. The descending sequence of this efficiency indicates a possible instability of the compound, which is evident from the decrease in the inhibition efficiency to 17.08% for 24 hours. As in Figure (20).

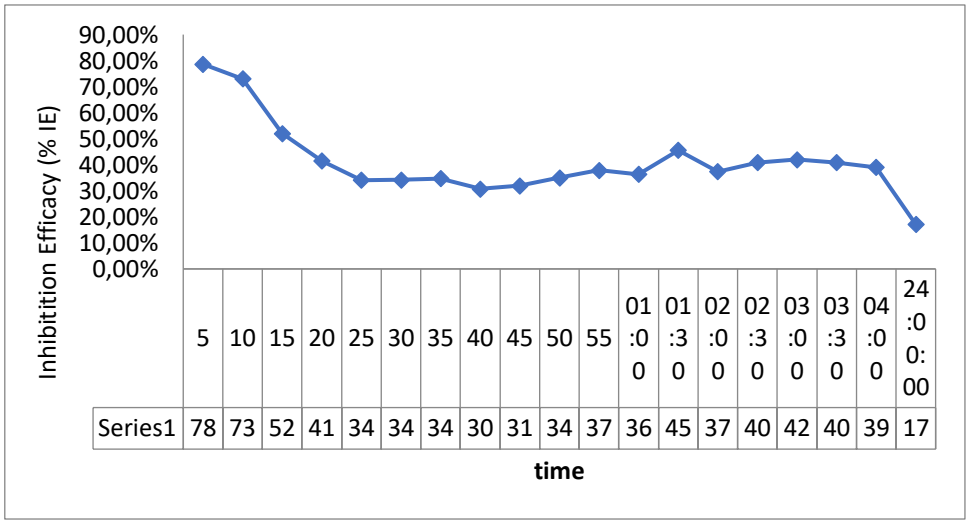

Figure 21. The percentage of the efficiency of inhibition of steel corrosion with time for the sample (3)

Compound (4) showed a progressive inhibition ability with time and the highest rate of inhibition was 72.9 at the first two hours, which indicates the effectiveness of the amine tricolor rings containing non-participating electrons on the nanoparticles, where the range of inhibition efficiency was 12.77-76.97. The activity is also attributed to the ability of the plates. The polarized nanoparticles are bound to the metal surface, which leads to their isolation from the acid medium.

The lowest inhibition value was 40% after 24 hours, and this indicates the relative stability of the compound. As in Figure (21).

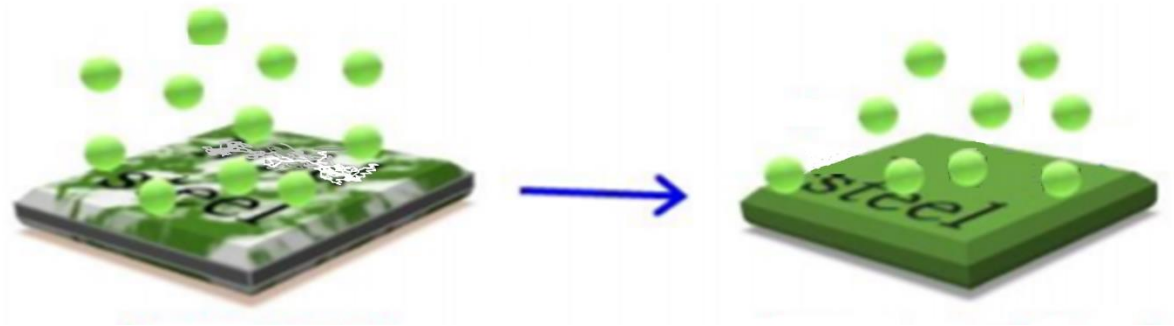

Figure 22. Stability of the compound

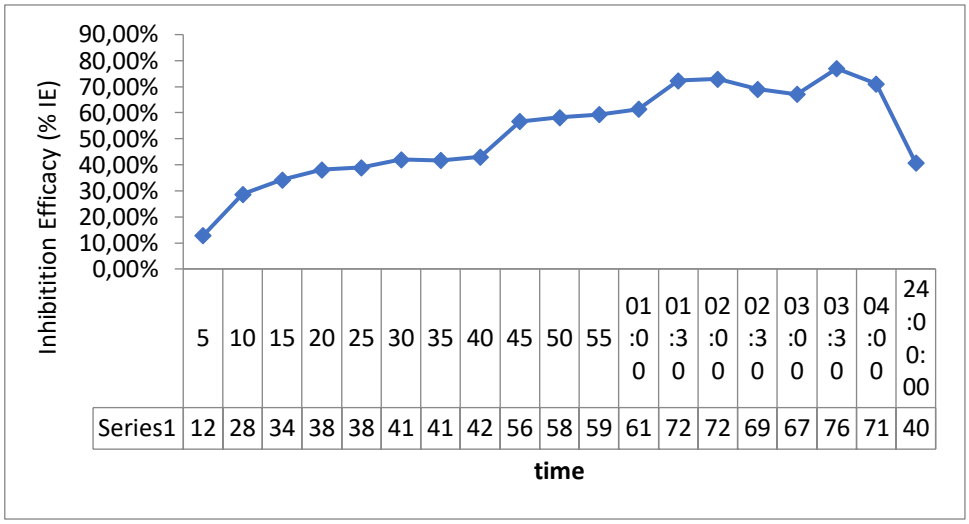

Figure 23. The percentage of the inhibition efficiency for steel corrosion with time for the sample (4)

Evaluation of the Biological Activity of Prepared Compounds

Due of their widespread disease-causing ability, these bacteria were selected for medical research. Their resistance to drugs varies as well [29, 30]. By monitoring the antibiotic levels and applying the etching procedure (130), it was possible to assess the bioavailability of some of the produced compounds [31,32]. Using the antibiotic amoxicillin as a control gene, the synthesized compounds were shown to be able to suppress the development of bacteria with varying proportions of Gram-positive and negative stains. It is based on tests from the World Health Organization and is utilized in Ministry of Health laboratories [33, 34]. As shown in table 3

Table 3. The development of bacteria

Comp. No.	K. pneumoniae Conc. mg/ml			Staph. epidermidis Conc. mg/ml		
	0.01	0.001	0.0001	0.01	0.001	0.0001
Comp5	23	15	10	20	14	7
Comp6	17	14	10	16	10	5
Comp7	21	18	12	19	15	10
Amoxicillin	25	20	15	22	19	15

4. Conclusion

The study successfully synthesized and characterized new imine graphene derivatives, confirming their structure through various analytical techniques. These derivatives exhibited notable antibacterial activity against both gram-positive and gram-negative bacteria. This suggests their potential for further development as antimicrobial agents, highlighting the effectiveness of graphene-based materials in biological applications.

REFERENCES

[1] R. S. Najm and G. H. Al-Somaidaie, "Carbonation and Preparation of Reduced Graphene Oxide Sheets from Cellulose," in *39th Pattaya International Conference on Advances in Chemical, Agriculture, Biology & Environment* (PCABE-22), Pattaya (Thailand), 2022, pp. 25-26.

[2] L. Dhiman and A. Dhamija, "Multifaceted Graphene: Novelty in Electronics," *International Journal of Advanced Research in Electrical, Electronics and Instrumentation Engineering*, vol. 3, no. 9, pp. 11807-11811, 2014.

[3] A. K. Geim and K. S. Novoselov, "The Rise of Graphene," *Nature Materials*, vol. 6, no. 3, pp. 183-191, 2007.

[4] G. Eda, G. Fanchini, and M. Chhowalla, "Large-Area Ultrathin Films of Reduced Graphene Oxide as a Transparent and Flexible Electronic Material," *Nature Nanotechnology*, vol. 3, no. 5, pp. 270-274, 2008.

[5] L. Shahriary and A. A. Athawale, "Graphene Oxide Synthesized by Using Modified Hummers Approach," *International Journal of Renewable Energy and Environmental Engineering*, vol. 2, no. 01, pp. 58-63, 2014.

[6] W. S. Hummers Jr. and R. E. Offeman, "Preparation of Graphitic Oxide," *Journal of the American Chemical Society*, vol. 80, no. 6, pp. 1339-1339, 1958.

[7] S. Di, Y. Qian, L. Wang, and Z. Li, "Biofunctionalization of Graphene and Its Two-Dimensional Analogues and Synthesis of Biomimetic Materials: A Review," *Journal of Materials Science*, pp. 1-29, 2022.

[8] F. Giannazzo, S. L. Avila, J. Eriksson, and S. Sonde, Eds., *Integration of 2D Materials for Electronics Applications*. MDPI, 2019.

[9] T. Schwamb, B. R. Burg, N. C. Schirmer, and D. Poulikakos, "An Electrical Method for the Measurement of the Thermal and Electrical Conductivity of Reduced Graphene Oxide Nanostructures," *Nanotechnology*, vol. 20, no. 40, pp. 405704, 2009.

[10] H. N. Naser, "Synthesis and Characterization of Ni (II), Cu (II), Co (II), Cr (II) and Fe (II) Metal Complexes of New 1, 3, 4-Triazole Derivative," *Iraqi National Journal of Chemistry*, vol. 17, no. 1, 2017.

[11] Q. Z. Khalaf, H. M. Saleh, and A. R. Mahmood, "Analytical Study for the Ability of Some Polymers to Gain Transitional Elements Ions in Different Temperature, pH Acidity Functional and Time Situations," 2009.

[12] A. R. Katritzky, Z. Wang, and R. J. Offerman, "S, S'- and S, N-Disubstituted Derivatives of 1, 3, 4-Thiadiazoledithiones," *Journal of Heterocyclic Chemistry*, vol. 27, no. 2, pp. 139-142, 1990.

[13] H. Bayrak, A. Demirbas, S. A. Karaoglu, and N. Demirbas, "Synthesis of Some New 1, 2, 4-Triazoles, Their Mannich and Schiff Bases and Evaluation of Their Antimicrobial Activities," *European Journal of Medicinal Chemistry*, vol. 44, no. 3, pp. 1057-1066, 2009.

[14] H. Choe, K. H. Nah, S. N. Lee, H. M. Lee, H. S. Lee, S. H. Jo, C. H. Leem, and Y. J. Jang, "Biochem. Biophys. Res. Commun.," vol. 344, pp. 72–78, 2006.

[15] Z. Rouifi, M. El Faydy, H. About, F. Benhiba, H. Ramsis, M. Boudalia, and B. Lakhrissi, "Electrochemical and Theoretical Studies of Adsorption and Corrosion Inhibition of Ethyl 5-Amino-1-((8-Hydroxyquinolin-5-yl) Methyl)-1H-1, 2, 3-Triazole-4-Carboxylate on Carbon Steel in Acidic Solution," *Journal of Materials and Environmental Science*, vol. 9, no. 2, pp. 453-465, 2018.

[16] M. J. Saleh and K. A. Al-Badrany, "Preparation, Characterization of New 2-Oxo Pyran Derivatives by AL2O3-OK Solid Base Catalyst and Biological Activity Evaluation," *Central Asian Journal of Medical and Natural Science*, vol. 4, no. 4, pp. 222-230, 2023.

[17] A. W. A. S. Talluh, M. J. Saleh, J. N. Saleh, K. Al-Badrany, and H. Mohammed Saleh Al-Jubori, "Preparation, Characterization, and Evaluation of the Biological Activity of New 2, 3-Dihydroquinazoline-4-One Derivatives," *European Journal of Modern Medicine and Practice*, vol. 4, no. 4, pp. 326-332, 2024.

[18] W. A. S. Talluh, "Preparation, Characterization, Evaluation of Biological Activity, and Study of Molecular Docking of Azetidine Derivatives," *Central Asian Journal of Medical and Natural Science*, vol. 5, no. 1, pp. 608-616, 2024.

[19] S. T. Abdul Wahed, "Preparation and Evaluation of Bacterial Activity and Study of the Crystalline Properties of Some 1, 3-Oxazepine-4, 7-Dione Derivatives," *Central Asian Journal of Theoretical and Applied Sciences*, vol. 5, no. 2, pp. 15-26, 2024.

[20] A. M. Al Rashidy, K. A. Al Badrany, and G. M. Al Garagoly, "Spectrophotometric Determination of Sulphamethoxazole Drug by New Pyrazoline Derived from 2, 4-Dinitro Phenyl Hydrazine," in *Materials Science Forum*, vol. 1002, pp. 350-359, 2020.

[21] M. M. Al-Tufah, S. S. Jasim, and K. A. Al-Badrany, "Synthesis and Antibacterial Evaluation of Some New Pyrazole Derivatives," *Prof. (Dr) R. K. Sharma*, vol. 20, no. 3, pp. 178, 2020.

[22] M. A. Krishnan, K. S. Aneja, A. Shaikh, S. Bohm, K. Sarkar, H. M. Bohm, and V. S. Raja, "Graphene-Based Anticorrosive Coatings for Copper," *RSC Advances*, vol. 8, no. 1, pp. 499-507, 2018.

[23] D. C. Singu, B. Joseph, V. Velmurugan, S. Ravuri, and A. N. Grace, "Combustion Synthesis of Graphene from Waste Paper for High Performance Supercapacitor Electrodes," *International Journal of Nanoscience*, vol. 17, no. 01n02, pp. 1760023, 2018.

[24] T. I. Younis, "Photometric Assay of L-Naphthyl Amine by Azo Coupling," Ph.D. dissertation, Mosul University, 1994.

[25] J. Song, X. Wang, and C. T. Chang, "Preparation and Characterization of Graphene Oxide," *Journal of Nanomaterials*, vol. 2014, no. 1, pp. 276143, 2014.

[26] K. S. Aneja, S. Bohm, A. S. Khanna, and H. M. Bohm, "Graphene-Based Anticorrosive Coatings for Cr (VI) Replacement," *Nanoscale*, vol. 7, no. 42, pp. 17879-17888, 2015.

[27] L. Zhang, Y. Li, H. Guo, H. Zhang, N. Zhang, T. Hayat, and Y. Sun, "Decontamination of U (VI) on Graphene Oxide/Al2O3 Composites Investigated by XRD, FT-IR and XPS Techniques," *Environmental Pollution*, vol. 248, pp. 332-338, 2019.

[28] L. Shahriary and A. A. Athawale, "Graphene Oxide Synthesized by Using Modified Hummers Approach," *International Journal of Renewable Energy and Environmental Engineering*, vol. 2, no. 01, pp. 58-63, 2014.

[29] J. N. Saleh and A. Khalid, "Synthesis, Characterization and Biological Activity Evaluation of Some New Pyrimidine Derivatives by Solid Base Catalyst AL2O3-OBa," *Central Asian Journal of Medical and Natural Science*, vol. 4, no. 4, pp. 231-239, 2023.

[30] M. J. Saleh, J. N. Saleh, and K. Al-Badrany, "Preparation, Characterization, and Evaluation of the Biological Activity of Pyrazoline Derivatives Prepared Using a Solid Base Catalyst," *European Journal of Modern Medicine and Practice*, vol. 4, no. 7, pp. 25-32, 2024.

[31] H. M. S. Al-Jubori, "Preparation and Characterization of Some 1, 3-Oxazepane-7, 4-Dione Derivatives and Evaluation of Their Biological Activity," *European Journal of Modern Medicine and Practice*, vol. 4, no. 4, pp. 333-343, 2024.

[32] S. A. Mohamed, M. S. Hussein, and K. A. Al-Badrany, "Synthesis and Characterization of Pyrazolines and Oxazapine Derivatives Using Chalcones as Precursor and Evaluation of Their Biological Activity," *Samarra Journal of Pure and Applied Science*, vol. 4, no. 4, 2022.

[33] A. W. A. S. Talluh, M. J. Saleh, and J. N. Saleh, "Preparation, Characterisation and Study of the Molecular Docking of Some Derivatives of the Tetrazole Ring and Evaluation of Their Biological Activity," *World of Medicine: Journal of Biomedical Sciences*, vol. 1, no. 7, pp. 15-23, 2024.

[34] H. Dalaf, M. J. Saleh, and J. N. Saleh, "Green Synthesis, Characterization, and Multifaceted Evaluation of Thiazolidinone Derivatives: A Study on Biological and Laser Efficacy," *European Journal of Modern Medicine and Practice*, vol. 4, no. 7, pp. 155-168, 2024.